frontiers in Environmental Science

ORIGINAL RESEARCH
published: 28 June 2018
doi: 10.3389/fenvs.2018.00065

In Situ X-Ray Tomography Imaging of Soil Water and Cyanobacteria From Biological Soil Crusts Undergoing Desiccation

*Estelle Couradeau[1,2†], Vincent J. M. N. L. Felde[3†], Dilworth Parkinson[4], Daniel Uteau[3], Alexis Rochet[4], Charlene Cuellar[4], Geoffrey Winegar[4], Stephan Peth[3], Trent R. Northen[1] and Ferran Garcia-Pichel[2,5]**

[1] Environmental Genomics and Systems Biology, Lawrence Berkeley National Laboratory, Berkeley, CA, United States, [2] School of Life Sciences, Arizona State University, Tempe, AZ, United States, [3] Department of Soil Science, University of Kassel, Witzenhausen, Germany, [4] Advanced Light Source, Lawrence Berkeley National Laboratory, Berkeley, CA, United States, [5] Center for Fundamental and Applied Microbiomics, Biodesign Institute, Arizona State University, Tempe, AZ, United States

OPEN ACCESS

Edited by:
Philippe C. Baveye,
AgroParisTech Institut des Sciences et Industries du Vivant et de L'environnement, France

Reviewed by:
Brandy Marie Toner,
University of Minnesota Twin Cities, United States
Aurore Degre,
University of Liège, Belgium

***Correspondence:**
Ferran Garcia-Pichel
ferran@asu.edu

[†] These authors have contributed equally to this work.

Specialty section:
This article was submitted to Soil Processes, a section of the journal Frontiers in Environmental Science

Received: 16 March 2018
Accepted: 08 June 2018
Published: 28 June 2018

Citation:
Couradeau E, Felde VJMNL, Parkinson D, Uteau D, Rochet A, Cuellar C, Winegar G, Peth S, Northen TR and Garcia-Pichel F (2018) In Situ X-Ray Tomography Imaging of Soil Water and Cyanobacteria From Biological Soil Crusts Undergoing Desiccation. Front. Environ. Sci. 6:65. doi: 10.3389/fenvs.2018.00065

Biological soil crusts (biocrusts) are millimeter-sized microbial communities developing on the topsoils of arid lands that cover some 12% of Earth's continental area. Biocrusts consist of an assemblage of mineral soil particles consolidated into a crust by microbial organic polymeric substances that are mainly produced by filamentous bundle-forming cyanobacteria, among which *Microcoleus vaginatus* is perhaps the most widespread. This cyanobacterium is the primary producer for, and main architect of biocrusts in many arid soils, sustaining the development of a diverse microbial community. Biocrusts are only active when wet, and spend most of their time in a state of desiccated quiescence, from which they can quickly recover upon wetting. Despite their ecological importance for arid ecosystems, little is known about the mechanisms that allow biocrust organisms to endure long periods of dryness while remaining viable for rapid resuscitation upon wetting. We had previously observed the persistence of significant rates of light-dependent carbon fixation in apparently dry biocrusts dominated by *M. vaginatus,* indicating that it may be able to remain hydrated against a background soil of very low water potential. One potential explanation for this may be that the abundant exopolysaccharide sheaths of *M. vaginatus* can preferentially retain moisture thus slowing the water equilibration with the surrounding soil allowing for extended activity periods. In order to test this hypothesis we aimed to develop methodologies to visualize and quantify the water dynamics within an undisturbed biocrust undergoing desiccation. We used synchrotron based X-ray microtomography and were able to resolve the distribution of air, liquid water, mineral particles and cyanobacterial bundles at the microscale. We could demonstrate the formation of steep, decreasing gradients of water content from the cyanobacterial bundle surface outward, while the bundle volume remained stable, as the local bulk water content decreased linearly, hence demonstrating a preferential retention of water in the microbes. Our data also suggest a transfer of hydration water from the EPS sheath material into the cyanobacterial filament as

desiccation progresses. This work demonstrates the value of X-ray tomography as a tool to study microbe-scale water redistribution in biocrusts.

Keywords: biocrust, *Microcoleus* sp., Synchrotron X-ray microtomography, water dynamics, desiccation experiment, EPS, cyanobacteria

INTRODUCTION

Biological soil crusts (biocrusts) are a community of micro and macroscopic organisms that develop in and on the surface layer of many soils worldwide (Belnap et al., 2016). They cover approximately 12% of Earth's terrestrial surface (Rodriguez-Caballero et al., 2018). Although they are widespread and can be found in all macroclimatic regions (Colesie et al., 2016), they are of special importance to dryland ecosystems because the biocrust organisms stabilize the soil against erosive forces through exopolysaccharide production (EPS) and increase soil fertility via the export of C and N to the soils they cover (Johnson et al., 2007; Strauss et al., 2012) and through the lixiviation of many other elements (Beraldi-Campesi et al., 2009). Biocrust organisms have developed various survival mechanisms in order to cope with a multitude of harsh environmental conditions (Pócs, 2009) that include high radiation (Garcia-pichel and Castenholz, 1991) and water scarcity (Rajeev et al., 2013).

Biocrusts are thought to have played an important role in shaping the Earth's terrestrial environments since the precambrian (Beraldi-Campesi and Garcia-Pichel, 2011; Beraldi-Campesi et al., 2014; Zhao et al., 2018). Mergelov et al. (2018) recently showed that the alteration of rocks by endolithic microbial communities is one likely pathway for the beginning of soils on Earth, and that the mechanisms of weathering and organic matter stabilization are strikingly similar to what can be observed in biocrusts nowadays. Present-day biocrusts mostly develop on bare (and often otherwise unconsolidated) substrate or young soils, triggering pedogenetic processes (Dümig et al., 2014). Depending on the various abiotic conditions, the conversion from bare substrate to the first successional stage of biocrust can take around 4 months (Ayuso et al., 2017). This first step is often the result of the activities of pioneer cyanobacteria such as *Microcoleus vaginatus,* a filamentous cyanobacterium that typically encompasses more than 25% of the early biocust microbial community (e.g., Kuske et al., 2012; Couradeau et al., 2016; Ayuso et al., 2017) particularly in areas with moderate temperature (Garcia-Pichel et al., 2013) and supports a community of heterotrophic bacteria and archaea through the release of a large variety of organic metabolites (Baran et al., 2015; Swenson et al., 2018). *M. vaginatus* not only enhances biocrust successional development through metabolic interactions but also directly enables the stabilization of soils particles and crust formation by binding soils particles to its large thallus (Garcia-Pichel and Wojciechowski, 2009), aided by the excretion of abundant exopolymeric substances (Rossi et al., 2012).

Biocrust biological activity is limited by the availability of liquid water. Upon rewetting *M. vaginatus* rapidly resumes respiration (within seconds), and photosynthetic activity (within minutes) (Rajeev et al., 2013). Genomic analyses have revealed that, upon drying, the cells accumulate intracellular compatible solutes as a means to withstand turgor pressure changes associate with desiccation (Rajeev et al., 2013; Murik et al., 2017). In previous studies of desiccation dynamics in *M. vaginatus*-dominated crusts, extended metabolic activities were detected in apparently dry biocrusts (soil water potential of −85 MPa) (Rajeev et al., 2013) suggesting the presence of a mechanism for sustained metabolic activity past the point of soil hydration. Unlike other bacteria, *M. vaginatus* does not differentiate spores or akinetes while entering dormancy, and yet it is one of the most desiccation resistant cyanobacteria in soil crusts (Fernandes et al., 2018). It is an often mentioned possibility that EPS production may contribute to desiccation resistance, although exact mechanisms or experimental evidence are still lacking. In this regard, it is generally thought that the bacterial EPS matrix may help to slow down cell re-hydration during rapid wetting of the soil, as well as retard the loss of water during desiccation (Volk et al., 2016; Adessi et al., 2018), thereby dampening the severity of osmotic shocks and helping attain gradual reactivation (see, for example, Or et al., 2007). The speed and extent of these processes is likely depending largely on EPS concentration, as well as their amphiphilic property (i.e., their monosaccharidic composition and the amount of proteins and lipids).

Here we hypothesized that the bundle-forming behavior of *M. vaginatus* and its EPS production may play a role in the adaptation of this organism to desiccation stress. To examine this with a new approach, we used synchrotron X-ray microtomography to track in a quantitative manner the dynamics of liquid water distribution in soil and microbes *in situ* in a drying biocrust.

MATERIALS AND METHODS

Sampling Site and Sample Preparation

The biocrust sample was collected in Moab, Utah (38°42′55″ N−109°41′33″ W) in a site dominated by light biocrusts, using a 6 cm diameter Petri dish (**Figures 1A,B**), allowed to air dry before being stored dry, in the dark in a repository. At the time of the experiment, a 4-mm diameter core was taken from the sample using the end of 1 mL pipette tip, and placed on the tomography sample holder. Some 300 μL of MilliQ water (Millipore Corp., USA) was added on top of the core to exceed water retention capacity and form a film of water on the surface. X-ray tomography scans (see below) were recorded sequentially for 3 h every 10 to 40 min as the sample dried.

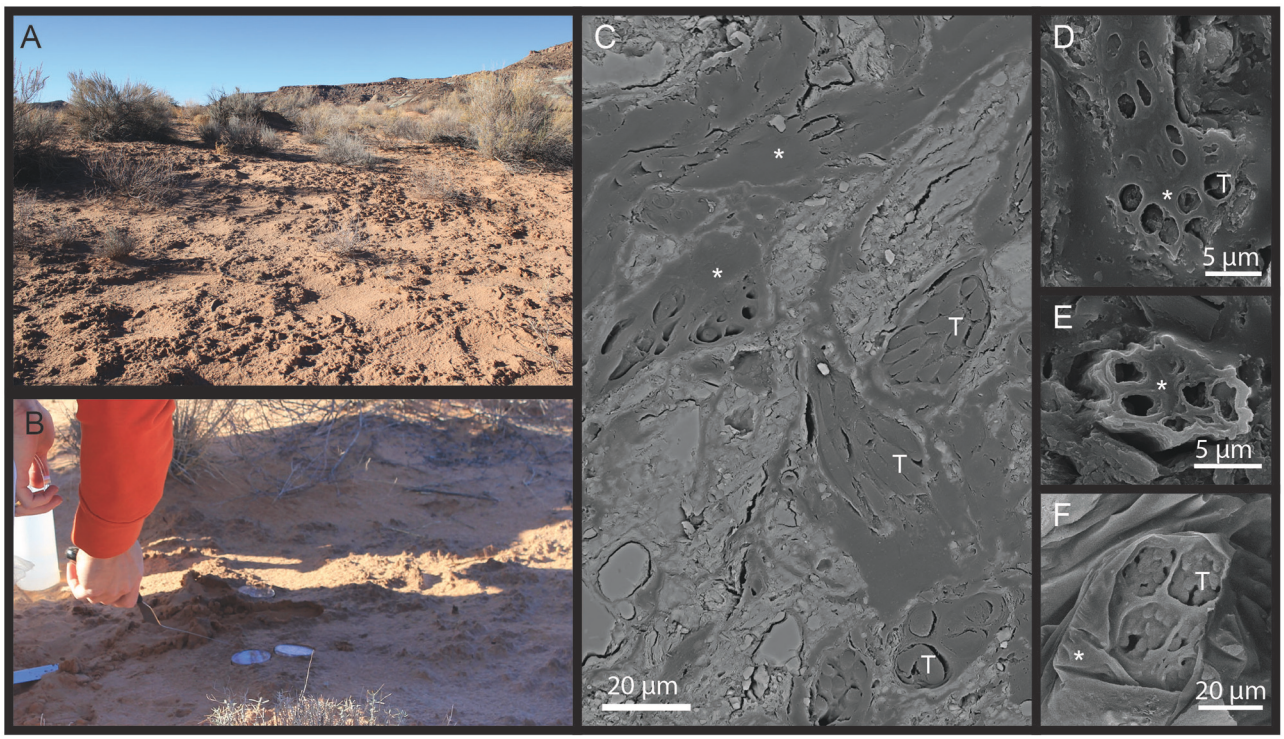

FIGURE 1 | (A) Aspect of the field site and **(B)** sampling illustration. **(C–F)** SEM pictures of a biocrust polished section using backscattered electron **(C)** and secondary electron **(D,E)** showing *Microcoleus* bundle (*) sheath material and cyanobacterial (T) trichomes *in situ*.

X-Ray Tomography Setup and Acquisition

X-ray tomography was performed at Beamline 8.3.2, the Hard X-ray Tomography beamline at the Advanced Light Source at Lawrence Berkeley National Laboratory (MacDowell et al., 2012). An X-ray energy of 25.7 keV was used, detection was accomplished with a 500 micron thick LuAG:Ce scintillator, a 5x Mitutoyo lens, and a PCO.edge sCMOS detector, yielding an effective voxel edge length of 1.3 µm. An exposure time of 250 ms per images was used, and the sample was rotated through 180 degrees while 1,025 images were collected for each scan. The temperature in the acquisition chamber was 24–27°C. The datasets analyzed for this study can be found in the Figshare repository https://doi.org/10.6084/m9.figshare.6447266.v1

Stack Reconstruction and Segmentation

Initial tomographic reconstruction was performed with image normalization and preprocessing implemented in FIJI/ImageJ (Schindelin et al., 2012) and tomographic reconstruction by the Octopus (XRE nv) software package. Subsequent reconstructions were performed using TomoPy (Gürsoy et al., 2014). The reconstructed stacks were processed and analyzed using MAVI (Modular Algorithms for Volume Images, Fraunhofer ITWM, Kaiserslautern) implemented in a Framework called ToolIP (Tool for Image Processing), where numerous analytical solutions can be automatized by means of flow processing charts. Custom python scripts developed for the ALS 8.3.2 beamline and used in this study can be found at https://bitbucket.org/berkeleylab/als-microct-python/src. A region of interest (ROI), containing a large cyanobacterial bundle, was cropped out for further analysis. The ROIs were filtered with a median filter with a window size of 9^3 voxels to smooth noise effects (**Figure 2**). To avoid ring artifacts and low contrast interfering with the segmentation, we had to segment the images in small steps. To do so, a sobel edge detection was used to exploit the phase contrast of the images. The sobel filter performs a spatial gradient computation that emphasizes regions of high spatial frequency that correspond to edges (Canny, 1986). A watershed segmentation was performed on the edge image, matching the solid phase (sand grains) and segmenting the image in small and more homogeneous pieces. Each watershed was then binarized using the bisection algorithm based on the method of Vogel and Kretzschmar (1996). A low threshold had to be set to identify voxels belonging to the solid phase (lowest gray values correspond to highest density materials) and an upper threshold for the gray values that could be assigned clearly to any phase. A voxel in the intermediate gray value range was assigned to the solid phase, if a neighbor voxel already belonged to it; otherwise it was assigned to the pore space. Both thresholds were calculated as the 10% deviation from the calculated Otsu-threshold (Otsu, 1979). This segmentation procedure allowed a low-noise segmentation without further intervention. During segmentation, most filaments were assigned to the solid phase, as was obvious after visual inspection. As those fragments were 1–2 orders of magnitude smaller in volume than most sand grains, we could label all foreground regions

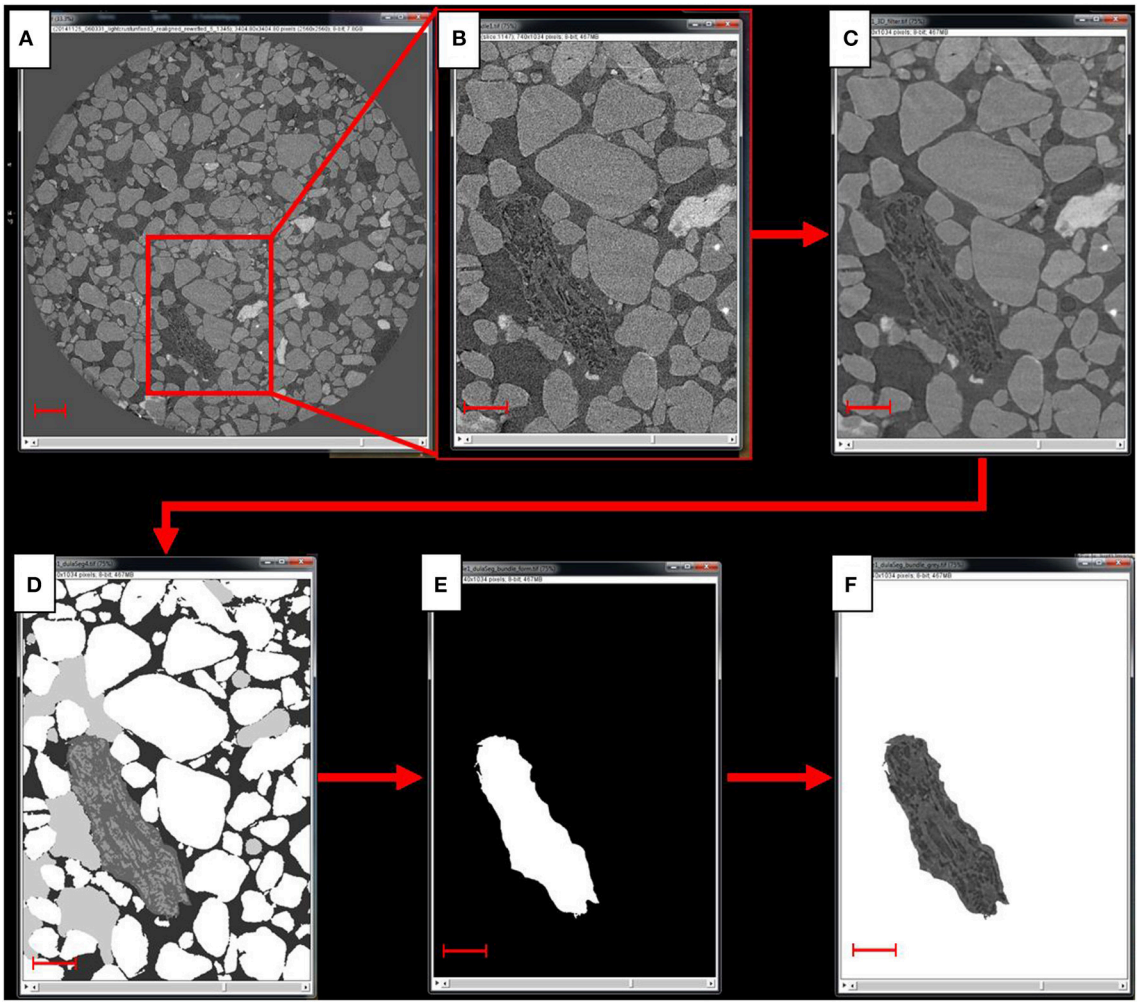

FIGURE 2 | Scheme of the image processing steps. From the reconstructed scan **(A)** a region of interest, or ROI, containing a large cyanobacterial bundle is cropped out **(B)**, to which then a 3D median filter is applied to reduce the noise **(C)**. Next, the image is segmented **(D)** and the segmented bundle **(E)** is used as a mask to cop out the bundle from the grayscale image of the ROI **(F)**. Scale bar in **(A)** equals 300 μm, scale bars in **(B–F)** equal 150 μm.

and eliminate the biggest classes by means of a 3D volume filter implemented in ToolIP-MAVI. Filament fragments but also fine sand grains then remained in the images. A closing operation was performed to merge filament fragments and aggregate them to form a structure that represents the bundle. The remaining fine sand grains were not close to the bundle; they remained more or less isolated from the rest and did not cluster by the effect of the closing operator. A volume filter was applied again, this time filtering all small objects (isolated grains) leaving only the mask of the bundle. A fillhole filter was finally applied to fill remaining holes in the bundle mask. The product of this procedure was used in the next steps. The isolation of the individual components of the cyanobacterial bundle (EPS sheath and cyanobacterial filaments) was performed by tracing them on a slice-by-slice basis using the Avizo (Avizo 3D software, ThermoFisher Scientific) segmentation editor interface, and these boundaries were slightly smoothed in the direction orthogonal to the slices on which tracing was performed, to eliminate inconsistencies.

Data Analysis

Distribution of Water and Air in the Microenvironment of the Cyanobacterial Bundle

In order to quantify the distribution of water and air close to the cyanobacterial bundle during desiccation, we analyzed the pore space in increasing distances to the bundle. For this, used the segmented bundle to create 8 masks, each of which had a width of 4 μm. This was achieved by applying a dilation algorithm in ImageJ, which inflates the bundle by one voxel. According to the 1.3 μm voxel resolution, we repeated the dilation thrice in order to get distance steps of 3.9 μm. We included the microenvironment around the bundle up to a distance of 32 μm (resulting in 8 masks at different distances from the bundle in steps of of approximately 4 μm). These masks were used

to crop out the the regions from the already segmented ROI. Subsequently, we counted the voxels that were segmented as solid phase, water and air filled pores and calculated the volume by multiplying voxel count by voxel volume.

Bundle Volume and Surface

The volume of the bundle was calculated by counting the total number of voxels and multiplying this number with the voxel volume. The surface area was measured with the "isosurface" feature of the well-established BoneJ algorithm for ImageJ (Doube et al., 2010). This feature uses marching cubes to create a triangular surface mesh and calculates the object surface as the sum of the areas of the triangles (Lorensen and Cline, 1987). Because a larger cube is less sensitve to small differences in surface roughness, we chose a comparatively large size for the marching cube (edge length: 15 voxel) in order to compensate for the different segmentation schemes that were used for different time points.

Scanning Electron Microscopy

A piece of biocrust from the same site was fixed in 2% glutaraldehyde overnight at 4°C before being rinsed 4 times with water. It was then dehydrated in successive bath of increasing concentration of ethanol (20–40–60–80–100%) for 7 min each under slow agitation. Spurr resin was used for impregnation, increasing concentration of resin in ethanol (25–50–75–100%) were used to incubate the sample for 3 h each under slow agitation. A final 100% resin bath was conducted overnight before the polymerisation step that consisted of 24 h incubation at 60°C in 100% resin. Finally the biocrust block was polished down to 0.5 micron using diamond paste and cloth, before being coated with platinum in a Technics Sputter Coater and imaged with a JEOL JSM6300 SEM equipped with a secondary electron detector and a XL30 Environmental FEG (FEI) equipped with a backscattered electron detector.

RESULTS

Suitability of Synchrotron Based X-Ray Microtomography to Track Water Flow *in Situ* in Biocrusts

Synchrotron based X-Ray microtomography was valuable for our purposes in that it is one of the few techniques that enables *in situ* visualization of a hydrated soil with enough contrast to resolve liquid water from air, while providing a spatial resolution sufficient to capture large cells (Aravena et al., 2011, 2014). Here we used it to image bundles of filamentous cyanobacteria *in situ* in a quartz dominated soil and their immediate surroundings. Classic SEM images of dried and embedded pieces of biocrust from the same source showed that individual, dry *Microcoleus vaginatus* filaments are ∼2–3 μm in diameter, assemble into a small bundle that further assembles in larger bundles, each unit being encased by EPS sheath material (**Figure 1**). We used these characteristics to recognize cyanobacterial bundles and their internal structure using synchrotron X-Ray microtomography, choosing one bundle of large size and following its behavior through desiccation. We were able to segment the interfaces between liquid water, gas phase, soil grains, and bundle as well as the inner components of the bundle, namely trichomes (cellular filaments) and EPS sheath material, (**Figure 2**); we could track them through a complete desiccation time series.

Analysis of the Microenvironment Around the Bundle

The analysis of the pore space around the bundle clearly shows a trend of decreasing water contents and porosity (i.e., more unconsolidated sand particles) with increasing distance away from the bundle (**Figure 3** and Table S1). This is true for the complete time sequence (42–91 min). During the initial phase of desiccation our data indicates the formation of a steep gradient in water availability decreasing away from bundle. The steepness of this gradient (i.e., the difference between the water content in the closest (0–4 μm) and farthest regions (28–32 μm) measured) decreases as the crust dries out. It is also evident from **Figure 3** that the total porosity (that is, the volume around the bundle that is not occupied by sand grains) increases, especially close to the bundle. It is likely that this pattern is caused by the physical shrinking of the bundle, i.e., space that was occupied by the bundle in the (swollen) hydrated state turns to air-filled pore space since sand grains remain at their initial position. This last observation demonstrates that the bundle sheath was not sufficiently strongly attached to the surrounding sand grains, so as to pull them along inwardly as the bundle shrunk (**Figure 4A**).

The Cyanobacterial Bundle Holds on to Water Throughout Desiccation

Expectedly, the volume and surface area of the bundle followed a similar dynamics. Unexpectedly, this dynamics had three differentiated phases. Bundle surface and volume remained relatively constant for the first hour, only to decrease noticeably between 61 and 91 min, then remaining again rather constant until the end of the experiment at 182 min (**Figure 4A**). This is especially noteworthy because the liquid water content in the full region of interests that we measured decreased much faster and more completely than the observed changes in bundle dimensions (**Figure 5**). The same dynamics of complete and linear desiccation could be observed in the water content of the region in the immediate vicinity of the bundle (0–32 μm; **Figure 4B**). This suggests the presence of a mechanism that retards water loss in the trichomes and sheath. Noting that hydrated microbial cells are some 80 percent water (by weight, and roughly volume), the final volume attained is at least 3 times larger than that expected of a completely dry bundle. Judging from the tri-phasic dynamics of shrinkage in the bundle, this mechanism may have at least two distinct components.

Bundle Shrinkage Dynamics and Possible Transfer of Water Between Sheath EPS and Cells

Overall the bundle shrunk by 20% in surface area and 33% in volume during the course of the experiment (see Table S2), however the EPS-sheath and the trichomes (cell filaments), had markedly different responses to drying (**Figure 5**). The volume

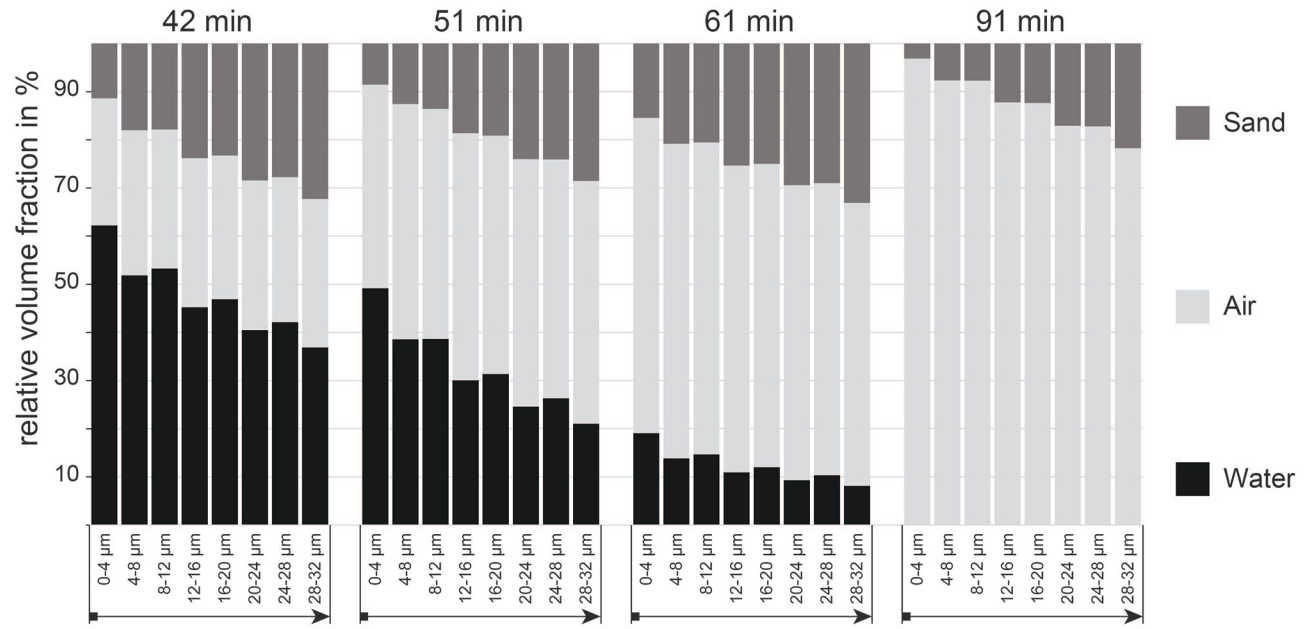

FIGURE 3 | Proportion of air and water filled pores, as well as volume occupied by sand grains in the 0–32 µm microenvironment around the cyanobacterial bundle measured in increments of 4 µm starting from the surface of the bundle.

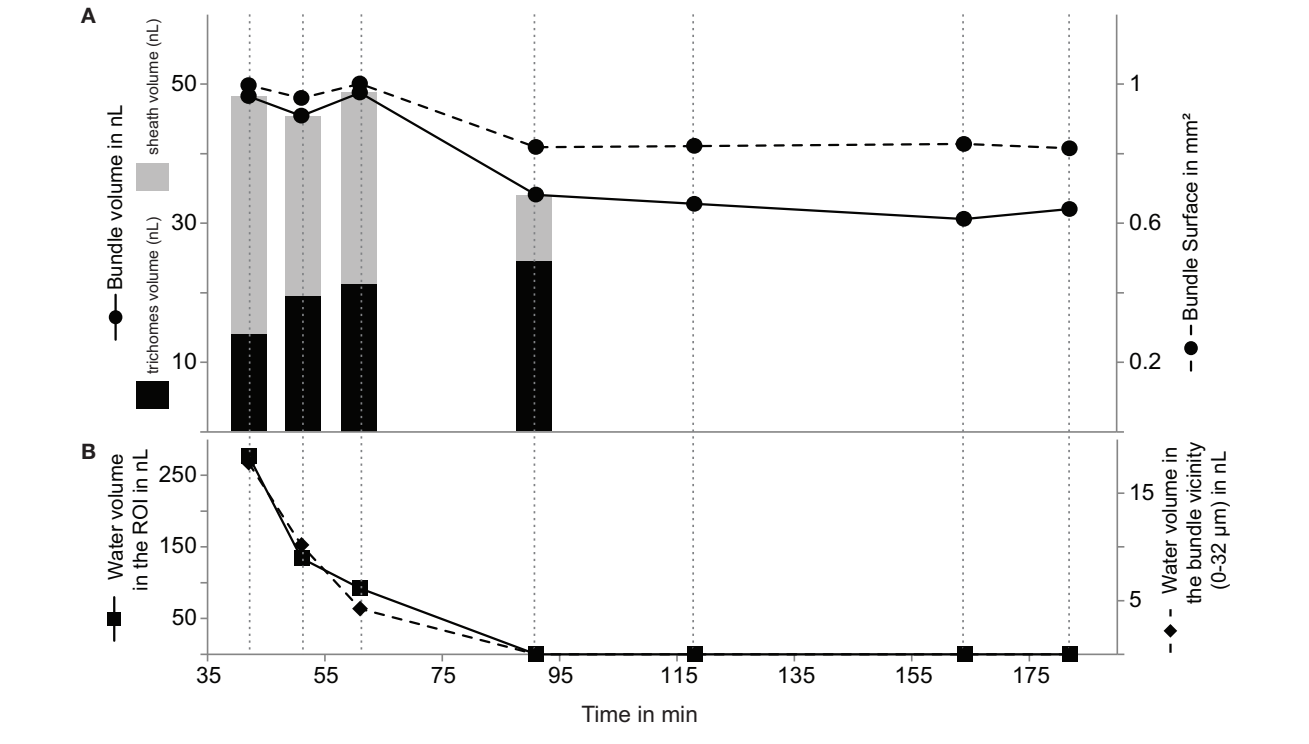

FIGURE 4 | Evolution of bundle volume and surface area **(A)** with decreasing local (0–32 µm from the bundle surface) and total (entire ROI) water content **(B)** from 42 to 182 min. The contribution of the trichomes (black) and sheath (gray) to the total bundle volume are plotted as bar plot for the first four time points **(A)**.

of EPS decreased significantly (by 70%) between 42 and 91 min, from 34.3 to 14.0 nL. During the same period, however, the volume of trichomes increased gradually from 9.5 to 24.6 nL (for a total increase of 75%) (Table S3). This suggests the intriguing possibility that a net water transfer occurred from the sheath material to the trichomes during this period. This ratio change

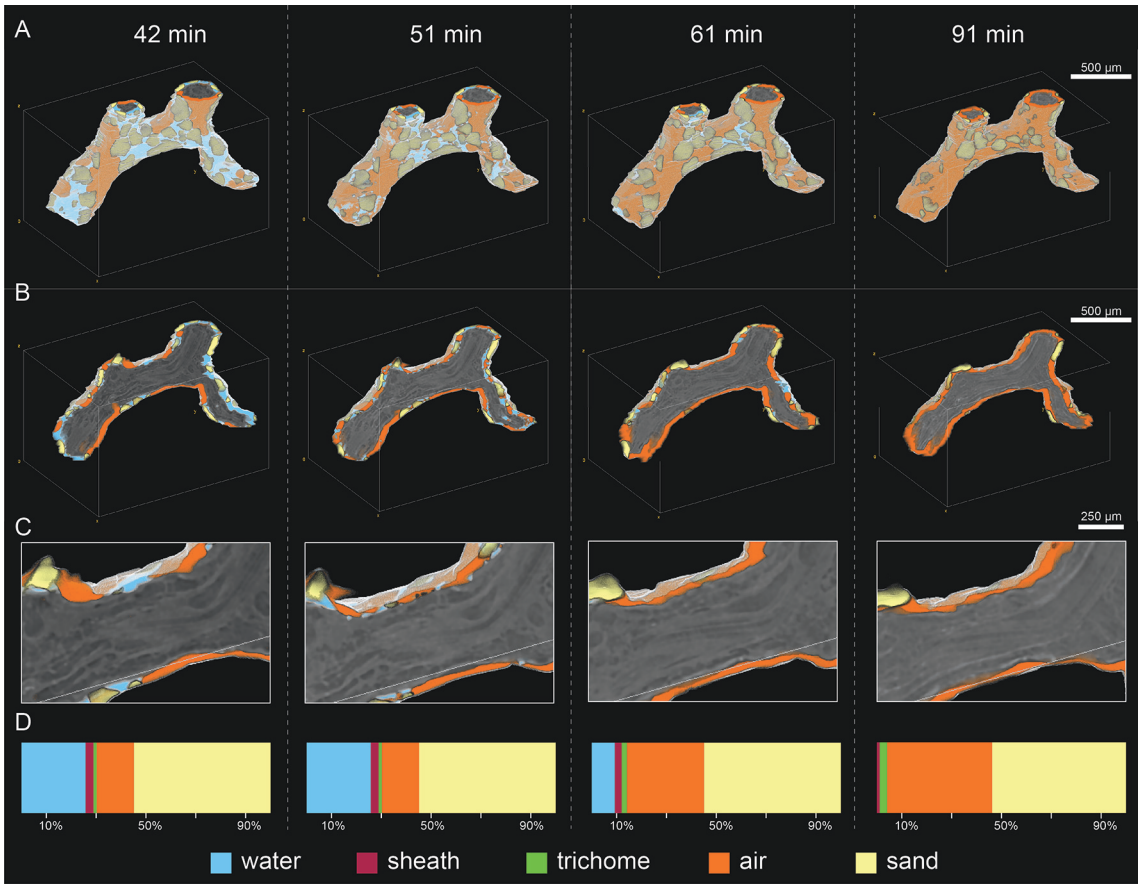

FIGURE 5 | Visualization of the full bundle **(A)**, a cross section of it **(B)** and a close-up cross section view **(C)** showing the distribution of water, air and sand in the 0–32 µm microenvironment around the bundle during desiccation from 42 to 91 min. Percent contribution of water, air, sand, trichome and sheath to the entire ROI are shown in panel **(D)**.

from the sheath-EPS to trichomes is also apparent on the cross section in **Figure 5C**, where one observes a transition from a swollen and hydrated bundle with many hydrated dark regions toward a dehydrated filament (with brighter color and thus, less water).

DISCUSSION

Preferential Water Retention Could Be Behind Sustained Metabolic Activity of *Microcoleus* in Dry Soils

The fact that the volume of the bundle is reduced to 66% of its initial size is likely a result of the loss of water during desiccation from 42 to 182 min. However, the data acquisition might not have captured the total desiccation process as one would expect a water content of 80% in fully hydrated stage. It is therefore possible that the bundle still contained water more than 90 min after the bulk soil was completely devoid of liquid water or that its volume was already less than the initial, fully hydrated at the first time point examined here. Over the course of the desiccation process, the volume ratio of sheath to trichomes changed gradually from 2.45 to 0.38 (**Figure 4A**, Table S3). The most likely explanation is that the trichomes absorbed water from the fully hydrated sheath EPS. A potential mechanism to drive the preferential transfer of sheath hydration water to the trichomes, rather than losing it to the pore space, may be a decreased intracellular water potential caused by the well-known accumulation of trehalose as a compatible solute in *Microcoleus vaginatus* as it undergoes desiccation (Rajeev et al., 2013). This accumulation can occur rather swiftly at the expense of intracellular glycogen reserves (Baran et al., 2013).

Water Holding Capacity of Sheath EPS Results in Effective Halting of Desiccation Fronts

Our results demonstrate for the first time directly that the cyanobacterial bundle and more particularly its sheath EPS material effectively remained hydrated while the surrounding soil pore regions were steadily drying. Although the nature of X-ray tomography limited our analyses to a single region in a single biocrust sample due to the work-intensive manual segmentation process (see methods), the observations that we made with our novel approach are consistent with the long-standing views on

the role of extracellular investments (sheaths capsules, diffuse EPS) in microbial adaptations to desiccation in general (see reviews by Potts, 1994; Rossi and De Philippis, 2015), and in soil crust systems in particular (Campbell, 1979; Or et al., 2007; Fischer et al., 2010). For example, our results also echo the observations made by Rosenzweig et al. (2012) and Adessi et al. (2018) who respectively showed that adding an EPS-analog to any soil increases water retention due to EPS water holding capacity and that preferential EPS extraction from a biocrust results in lessened water retention. These observations were also confirmed by Colica et al. (2014) who described a positive correlation of EPS and water retention in newly formed biocrusts associated with a significantly negative correlation of EPS concentration and hydraulic conductivity. One should be careful, however, in trying to explain the properties of crust EPS, from what one sees in a single species, namely *M. vaginatus*, given that crusts contain a large variety of mucus producing microbes, not only cyanobacteria but many of the bacterial heterotrophs as well (i.e S*phingomonas mucosissima;* Reddy and Garcia-Pichel, 2007).

Bundle-Mineral Particle Interaction

Our observation that the sheath EPS of *M. vaginatus* may not be strongly adherent to the sand grains can help shed light on previous studies. The fact that the sand grain are pulled away from the bundle during dry-down could be explained by their attachment to matrix EPS rather than sheath EPS, another type of biocrust EPS that would also shrink upon dry-up (Rossi et al., 2017). Rossi et al. (2012) used a non-invasive method for the extraction of EPS and noticed a change in the albedo and in the infiltrability of a variety of crusts after the treatment. This was hypothesized to be the outcome of the collapse of larger pores after the EPS were removed. In order to test this hypothesis, Felde et al. (2016) extracted the EPS from BSCs of four different ecosystems and scanned them before and after the extraction with a high-resolution μCT to quantify structural changes. Unexpectedly, no significant effect of the EPS extraction on the properties of the pore system was found in that study. However, this is consistent with the findings of our present study, where we could show that the EPS from the sheath did not strongly adhere to the sand grains, as their proportion in the microenvironment of the bundle decreased with desiccation, meaning that they stayed in place, while the bundle reduced its volume.

Benefits and Limitations of X-Ray Microtomography for Soil Microbiome Research

X-ray microtomography has been used for more than two decades to elucidate soil properties, such as pore space geometry and connectivity (Spanne et al., 1993; Peth et al., 2008; Ma et al., 2015). The main value of this technique applied to soil studies is that it requires little to no sample preparation, preserves the soil structure, is non-invasive, and enables the imaging of the interior of micrometer to centimeter size samples composed of any mineral phase. However, in the case of synchrotron-CT, it uses specialized facilities that require significant organizational effort before experimentation. It also requires intense computational efforts combined with expert decision making for segmentation, although these may in the future benefit from improved procedures based on machine learning. Menon et al. (2011) used it for the first time in dry biocrusts, imaging samples from the Kalhari desert to map pore structure and predict pathways of water flow. Neutron tomography (e.g., Tötzke et al., 2017), and X-Ray microtomography are the only techniques that allow resolution of *in situ* water flows (Aravena et al., 2014; Pot et al., 2015), but the spatial resolution of the former (∼10–100 microns) might not be best suited to resolve microbial cells or colonies whose size is typically an order of magnitude smaller. The spatial resolution of X-ray tomography, by contrast, can go down to $<1\,\mu m$ provided that samples are small enough (the voxel resolution is approximately in the order of 1/1,000 of the sample diameter, 1.3 micron in the present study), making it appropriate to advance soil microbiome research at relevant microbial scales. Beyond examination of soil water, Voltolini et al. (2017) for example, characterized the porosity of two soil aggregates to determine the volume accessible to microbial cells of differing size, making it possible to predict how favorable a soil could be to host connected microbial colonies. Further, using osmium to stain organic matter, Peth et al. (2014) were able to localize soil organics within soil aggregates. Here, taking advantage of the biocrust soil system, in which microbial communities are concentrated in the topmost millimeters of soil, and host large bundles of filamentous cyanobacteria, we could segment a large microbial colony (a bundle) and resolve its internal structure. Another point to take into account when considering applying this technique to microbial ecology in general is that even though nominally non destructive, the use of hard X-rays may damage the sample (in particular its biological component). It was shown for instance that it can induce death of large population of selected groups of organisms directly after the scan (Fischer et al., 2013) or have negligible effect depending the dose of X-ray and scan duration (Schmidt et al., 2015). In our case it prevented the cyanobacterium to migrate to the biocrust surface upon rewetting after the experiment (data not shown), which they invariably do when healthy (Pringault and Garcia-Pichel, 2004) suggesting that the imaging process may have impaired their physiology.

Bundle Forming Behavior

The bundle forming behavior clearly limits the ability of light and nutrients to reach cyanobacterial trichomes inside of this crowded conformation, which could be particularly detrimental in an environment where these resources are only available during limited pulses of activity. This seems counter-intuitive, and suggests that bundle-formation must bring about significant adaptive value in some other form. It was already shown that the bundle association behavior serves as an adaptation to soil stabilization (Garcia-Pichel and Wojciechowski, 2009) allowing the establishment of microbial colonies on an otherwise mobile substrate, a feat that is size dependent and unattainable to single filaments. Our work here further suggests that the amount of sheath EPS could be critical to buffer local water dehydration and transfer water to the trichomes. In this sense, bundle formation, i.e., sheath sharing behavior, in an activity

limited environment may also be an adaptive trade-off that favors sustained *Microcoleus* sp. populations in arid lands.

CONCLUSIONS

Our study looked in detail at the process of desiccation of one single bundle inside an early successional stage biocrust. We could show that the bundle remains hydrated while the surroundings are drying, and that the EPS-sheath represents a buffer zone able to redistribute its hydration water to the cyanobacterial cells. We observed that the sand particles were apparently not strongly attached to the bundle since they did not stay close to the bundle through desiccation, increasing pore space around the bundle as desiccation progresses. Our study was somewhat limited by the fact that manual data treatment was required to distinguish liquid water from air and sheath from trichome phases. However, we hope that this study will serve as a pioneer for additional studies, and that machine learning approaches will provide an avenue to improve synchrotron X-ray microtomography approached to the study of water/microbes interactions in soils crusts and other relevant microbial systems.

AUTHOR CONTRIBUTIONS

EC, TN, and FG-P designed the experiment. EC and FG-P collected the sample, acquired the SEM images and wrote the paper. VF analyzed the data and wrote the paper. EC, FG-P, and DP conducted the CT-scans at the Advanced Light Source (LBNL). DU, SP, AR, GW, and CC analyzed the data.

ACKNOWLEDGMENTS

This research used resources of the Advanced Light Source, which is a DOE Office of Science User Facility under contract no. DE-AC02-05CH11231. This work was supported by a grant of the National Science Foundation DEB-0717164 to F.G-P, and by the US Department of Energy Office of Science and through the US Department of Energy Office of Science, Office of Biological and Environmental Research Early Career Program (award to TN) under contract to Lawrence Berkeley National Laboratory number and DE-AC02-05CH11231. EC was funded from the European Union's Seventh Framework Program for research, technological development and demonstration under grant agreement no 328530. EC would like to thank Ariane Couradeau Delattre for her support through data acquisition. VF thanks Aaron Kaplan for a very fruitful discussion on the mechanisms governing desiccation tolerance.

SUPPLEMENTARY MATERIAL

The Supplementary Material for this article can be found online at: https://www.frontiersin.org/articles/10.3389/fenvs.2018.00065/full#supplementary-material

REFERENCES

Adessi, A., Cruz de Carvalho, R., De Philippis, R., Branquinho, C., and Marques da Silva, J. (2018). Microbial extracellular polymeric substances improve water retention in dryland biological soil crusts. *Soil Biol. Biochem.* 116, 67–69. doi: 10.1016/j.soilbio.2017.10.002

Aravena, J. E., Berli, M., Ghezzehei, T. A., and Tyler, S. W. (2011). Effects of root-induced compaction on rhizosphere hydraulic properties–X-ray microtomography imaging and numerical simulations. *Environ. Sci. Technol.* 45, 425–431. doi: 10.1021/es102566j

Aravena, J. E., Berli, M., Ruiz, S., Suárez, F., Ghezzehei, T. A., and Tyler, S. W. (2014). Quantifying coupled deformation and water flow in the rhizosphere using X-ray microtomography and numerical simulations. *Plant Soil* 376, 95–110. doi: 10.1007/s11104-013-1946-z

Ayuso, S. V., Silva, A. G., Nelson, C., Barger, N. N., and Garcia-Pichel, F. (2017). Microbial nursery production of high-quality biological soil crust biomass for restoration of degraded dryland soils. *Appl. Environ. Microbiol.* 83, 1–16. doi: 10.1128/AEM.02179-16

Baran, R., Brodie, E. L., Mayberry-Lewis, J., Hummel, E., Da Rocha, U. N., Chakraborty, R., et al. (2015). Exometabolite niche partitioning among sympatric soil bacteria. *Nat. Commun.* 6, 8289. doi: 10.1038/ncomms9289

Baran, R., Ivanova, N. N., Jose, N., Garcia-Pichel, F., Kyrpides, N. C., Gugger, M., et al. (2013). Functional genomics of novel secondary metabolites from diverse cyanobacteria using untargeted metabolomics. *Mar. Drugs* 11, 3617–3631. doi: 10.3390/md11103617

Belnap, J., Weber, B., and Büdel, B. (2016). "Biological soil crusts as an organizing principle in drylands," in *Biological Soil Crusts: An Organizing Principle in Drylands*, eds B. Weber, B. Büdel, and J. Belnap (Cham: Springer International Publishing), 3–13.

Beraldi-Campesi, H., Farmer, J. D., and Garcia-Pichel, F. (2014). Modern terrestrial sedimentary biostructures and their fossil analogs in mesoproterozoic subaerial deposits. *Palaios* 29, 45–54. doi: 10.2110/palo.2013.084

Beraldi-Campesi, H., and Garcia-Pichel, F. (2011). The biogenicity of modern terrestrial roll-up structures and its significance for ancient life on land. *Geobiology* 9, 10–23. doi: 10.1111/j.1472-4669.2010.00258.x

Beraldi-Campesi, H., Hartnett, H. E., Anbar, A., Gordon, G. W., and Garcia-Pichel, F. (2009). Effect of biological soil crusts on soil elemental concentrations: implications for biogeochemistry and as traceable biosignatures of ancient life on land. *Geobiology* 7, 348–359. doi: 10.1111/j.1472-4669.2009.00204.x

Campbell, S. E. (1979). Soil stabilization by a prokaryotic desert crust: implications for Precambrian land biota. *Orig. Life* 9, 335–348. doi: 10.1007/BF00926826

Canny, J. (1986). A computational approach to edge detection. *IEEE Trans. Pattern Anal. Mach. Intell.* 8, 679–698.

Colesie, C., Felde, V. J. M. N. L., and Büdel, B. (2016). "Composition and macrostructure of biological soil crusts," in *Biological Soil Crusts: An Organizing Principle in Drylands*, eds B. Weber, B. Büdel, and J. Belnap (Cham: Springer International Publishing), 159–172.

Colica, G., Li, H., Rossi, F., Li, D., Liu, Y., and Philippis, R. (2014). Microbial secreted exopolysaccharides affect the hydrological behavior of induced biological soil crusts in desert sandy soils. *Soil Biol. Biochem.* 68, 62–70. doi: 10.1016/j.soilbio.2013.09.017

Couradeau, E., Karaoz, U., Lim, H. C., Nunes da Rocha, U., Northen, T., Brodie, E., et al. (2016). Bacteria increase arid-land soil surface temperature through the production of sunscreens. *Nat. Commun.* 7:10373. doi: 10.1038/ncomms10373

Doube, M., Kłosowski, M. M., Arganda-Carreras, I., Cordelières, F. P., Dougherty, R. P., Jackson, J. S., et al. (2010). BoneJ: free and extensible bone image analysis in ImageJ. *Bone* 47, 1076–1079. doi: 10.1016/j.bone.2010.08.023

Dümig, A., Veste, M., Hagedorn, F., Fischer, T., Lange, P., Spröte, R., et al. (2014). Organic matter from biological soil crusts induces the initial formation of

sandy temperate soils. *CATENA* 122, 196–208. doi: 10.1016/j.catena.2014.06.011

Felde, V. J. M. N. L., Rossi, F., Colesie, C., Uteau-Puschmann, D., Horn, R., Felix-Henningsen, P., et al. (2016). Pore characteristics in biological soil crusts are independent of extracellular polymeric substances. *Soil Biol. Biochem.* 103, 294–299. doi: 10.1016/j.soilbio.2016.08.029

Fernandes, V, Machado de Lima, N, Roush, D, Collins, S, Rutgers, J, and Garcia-Pichel, F (2018). Exposure to predicted precipitation patterns decrease population size and alter community structure of cyanobacteria in biological soil crusts from the Chihuahuan Desert. *Environm. Microbiol.* 20, 259–269. doi: 10.1111/1462-2920.13983

Fischer, D., Pagenkemper, S., Nellesen, J., Peth, S., Horn, R., and Schloter, M. (2013). Influence of non-invasive X-ray computed tomography (XRCT) on the microbial community structure and function in soil. *J. Microbiol. Methods* 93, 121–123. doi: 10.1016/j.mimet.2013.02.009

Fischer, T., Veste, M., Wiehe, W., and Lange, P. (2010). Water repellency and pore clogging at early successional stages of microbiotic crusts on inland dunes, Brandenburg, NE Germany. *CATENA* 80, 47–52. doi: 10.1016/j.catena.2009.08.009

Garcia-pichel, F., and Castenholz, R. W. (1991). Characterizaton and biological implications of scytonemin, a cyanobacterial sheath pigment. *J. Phycol.* 409, 395–409.

Garcia-Pichel, F., Loza, V., Marusenko, Y., Mateo, P., and Potrafka, R. M. (2013). Temperature drives the continental-scale distribution of key microbes in topsoil communities. *Science* 340, 1574–1577. doi: 10.1126/science.1236404

Garcia-Pichel, F., and Wojciechowski, M. F. (2009). The evolution of a capacity to build supra-cellular ropes enabled filamentous cyanobacteria to colonize highly erodible substrates. *PLoS ONE* 4:e7801. doi: 10.1371/journal.pone.0007801

Gürsoy, D., De Carlo, F., Xiao, X., and Jacobsen, C. (2014). TomoPy: a framework for the analysis of synchrotron tomographic data. *J. Synchrotron Radiat.* 21, 1188–1193. doi: 10.1107/S1600577514013939

Johnson, SL, Neuer, S, and Garcia-Pichel, F (2007). Export of nitrogenous compounds due to incomplete cycling within biological soil crusts of arid lands. *Environ Microbiol.* 9, 680–689. doi: 10.1111/j.1462-2920.2006.01187.x

Kuske, C. R., Yeager, C. M., Johnson, S., Ticknor, L. O., and Belnap, J. (2012). Response and resilience of soil biocrust bacterial communities to chronic physical disturbance in arid shrublands. *ISME J.* 6, 886–897. doi: 10.1038/ismej.2011.153

Lorensen, W. E., and Cline, H. E. (1987). Marching cubes: a high resolution 3D surface construction algorithm. *ACM Siggr. Comput. Graph.* 21, 163–169. doi: 10.1145/37401.37422

Ma, R., Cai, C., Li, Z., Wang, J., Xiao, T., Peng, G., et al. (2015). Evaluation of soil aggregate microstructure and stability under wetting and drying cycles in two Ultisols using synchrotron-based X-ray micro-computed tomography. *Soil Tillage Res.* 149, 1–11. doi: 10.1016/j.still.2014.12.016

MacDowell, A. A., Parkinson, D. Y., Haboub, A., Schaible, E., Nasiatka, J. R., Yee, C. A., et al. (2012). "X-ray micro-tomography at the advanced light source," in *Proceedings of SPIE 8506, Developments in X-Ray Tomography* VIII 8506 (San Diego, CA).

Menon, M., Yuan, Q., Jia, X., Dougill, A. J., Hoon, S. R., Thomas, A. D., et al. (2011). Assessment of physical and hydrological properties of biological soil crusts using X-ray microtomography and modeling. *J. Hydrol.* 397, 47–54. doi: 10.1016/j.jhydrol.2010.11.021

Mergelov, N., Mueller, C. W., Prater, I., Shorkunov, I., Dolgikh, A., Zazovskaya, E., et al. (2018). Alteration of rocks by endolithic organisms is one of the pathways for the beginning of soils on Earth. *Sci. Rep.* 8:3367. doi: 10.1038/s41598-018-21682-6

Murik, O., Oren, N., Shotland, Y., Raanan, H., Treves, H., Kedem, I., et al. (2017). What distinguishes cyanobacteria able to revive after desiccation from those that cannot: the genome aspect: desiccation resistance genes in cyanobacteria. *Environ. Microbiol.* 19, 535–550. doi: 10.1111/1462-2920.13486

Or, D., Phutane, S., and Dechesne, A. (2007). Extracellular polymeric substances affecting pore-scale hydrologic conditions for bacterial activity in unsaturated soils. *Vadose Zone J.* 6, 298. doi: 10.2136/vzj2006.0080

Otsu, N. (1979). A threshold selection method from gray-level histograms. *IEEE Trans. Syst. Man Cybern.* 9, 62–66. doi: 10.1109/TSMC.1979.4310076

Peth, S., Chenu, C., Leblond, N., Mordhorst, A., Garnier, P., Nunan, N., et al. (2014). Localization of soil organic matter in soil aggregates using synchrotron-based X-ray microtomography. *Soil Biol. Biochem.* 78, 189–194. doi: 10.1016/j.soilbio.2014.07.024

Peth, S., Horn, R., Beckmann, F., Donath, T., Fischer, J., and Smucker, A. J. M. (2008). Three-dimensional quantification of intra-aggregate pore-space features using synchrotron-radiation-based microtomography. *Soil Sci. Soc. Am. J.* 72, 897. doi: 10.2136/sssaj2007.0130

Pócs, T. (2009). Cyanobacterial crust types, as strategies for survival in extreme habitats. *Acta Bot. Hung.* 51, 147–178. doi: 10.1556/ABot.51.2009.1-2.16

Pot, V., Peth, S., Monga, O., Vogel, L. E., Genty, A., Garnier, P., et al. (2015). Three-dimensional distribution of water and air in soil pores: comparison of two-phase two-relaxation-times lattice-Boltzmann and morphological model outputs with synchrotron X-ray computed tomography data. *Adv. Water Resour.* 84, 87–102. doi: 10.1016/j.advwatres.2015.08.006

Potts, M. (1994). Desiccation tolerance of prokaryotes. *Microbiol. Rev.* 58, 755–805. doi: 10.1093/icb/45.5.800

Pringault, O., and Garcia-Pichel, F. (2004). Hydrotaxis of cyanobacteria in desert crusts. *Microb. Ecol.* 47, 366–373. doi: 10.1007/s00248-002-0107-3

Rajeev, L., da Rocha, U. N., Klitgord, N., Luning, E. G., Fortney, J., Axen, S. D., et al. (2013). Dynamic cyanobacterial response to hydration and dehydration in a desert biological soil crust. *ISME J.* **7**, 2178–2191. doi: 10.1038/ismej.2013.83

Reddy, G. S. N., and Garcia-Pichel, F. (2007). *Sphingomonas mucosissima* sp. nov. and *Sphingomonas desiccabilis* sp. nov., from biological soil crust in the Colorado Plateau, USA. *Int. J. Syst. Evol. Microbiol.* 57, 1028–1034. doi: 10.1099/ijs.0.64331-0

Rodriguez-Caballero, E., Belnap, J., Büdel, B., Crutzen, P. J., Andreae, M. O., Pöschl, U., et al. (2018). Dryland photoautotrophic soil surface communities endangered by global change. *Nat. Geosci.* **11**, 85–189. doi: 10.1038/s41561-018-0072-1

Rosenzweig, R., Shavit, U., and Furman, A. (2012). Water retention curves of biofilm-affected soils using xanthan as an analogue. *Soil Sci. Soc. Am. J.* 76:61. doi: 10.2136/sssaj2011.0155

Rossi, F., and De Philippis, R. (2015). Role of cyanobacterial exopolysaccharides in phototrophic biofilms and in complex microbial mats. *Life* 5, 1218–1238. doi: 10.3390/life5021218

Rossi, F., Mugnai, G., and de Philippis, R. (2017). Complex role of the polymeric matrix in biological soil crusts. *Plant Soil*. doi: 10.1007/s11104-017-3441-4. [Epub ahead of print].

Rossi, F., Potrafka, R. M., Pichel, F. G., and De Philippis, R. (2012). The role of the exopolysaccharides in enhancing hydraulic conductivity of biological soil crusts. *Soil Biol. Biochem.* 46, 33–40. doi: 10.1016/j.soilbio.2011.10.016

Schindelin, J., Arganda-Carreras, I., Frise, E., Kaynig, V., Longair, M., Pietzsch, T., et al. (2012). Fiji: an open-source platform for biological-image analysis. *Nat. Methods* 9, 676–682. doi: 10.1038/nmeth.2019

Schmidt, H., Vetterlein, D., Köhne, J.M., and Eickhorst, T. (2015). Negligible effect of X-ray μ-CT scanning on archaea and bacteria in an agricultural soil. *Soil Biol. Biochem.* 84, 21–27 doi: 10.1016/j.soilbio.2015.02.010

Spanne, P., Jones, K. W., Prunty, L. D., and Anderson, S. H. (1993). "Potential applications of synchrotron computed microtomography to soil science," in *1992 Annual Meetings of the American Society of Agronomy, Crop Science Society of America, and Soil Science Society of America* (Minneapolis, MN).

Strauss, S. L., Day, T. A., and Garcia-Pichel, F. (2012). Nitrogen cycling in desert biological soil crusts across biogeographic regions in the southwestern United States. *Biogeochemistry* 108, 171–182. doi: 10.1007/s10533-011-9587-x

Swenson, T. L., Karaoz, U., Swenson, J. M., Bowen, B. P., and Northen, T. R. (2018). Linking soil biology and chemistry in biological soil crust using isolate exometabolomics. *Nat. Commun.* 9:19. doi: 10.1038/s41467-017-02356-9

Tötzke, C., Kardjilov, N., Manke, I., and Oswald, S. E. (2017). Capturing 3D water flow in rooted soil by ultra-fast neutron tomography. *Sci. Rep.* 7, 1–9. doi: 10.1038/s41598-017-06046-w

Vogel, H. J., and Kretzschmar, A. (1996). Topological characterization of pore space in soil — sample preparation and digital image-processing. *Geoderma* 73, 23–38. doi: 10.1016/0016-7061(96)00043-2

Volk, E., Iden, S. C., Furman, A., Durner, W., and Rosenzweig, R. (2016). Biofilm effect on soil hydraulic properties: experimental investigation using soil-grown real biofilm: HYDRAULIC PROPERTIES OF BIOFILM AMENDED SOIL. *Water Resour. Res.* 52, 5813–5828. doi: 10.1002/2016WR018866

Voltolini, M., Taş, N., Wang, S., Brodie, E. L., and Ajo-Franklin, J. B. (2017). Quantitative characterization of soil micro-aggregates: new opportunities from sub-micron resolution synchrotron X-ray microtomography. *Geoderma* 305, 382–393. doi: 10.1016/j.geoderma.2017.06.005

Zhao, M., Reinhard, C. T., and Planavsky, N. J. (2018). Terrestrial methane fluxes and Proterozoic climate. *Geology* 46, 1–4. doi: 10.1130/G39502.1

Conflict of Interest Statement: The authors declare that the research was conducted in the absence of any commercial or financial relationships that could be construed as a potential conflict of interest.